THE JOURNAL OF PHYSICAL CHEMISTRY B

Article

Cite This: J. Phys. Chem. B 2018, 122, 1026−1036

pubs.acs.org/JPCB

Binding Mechanisms of Electron Transport Proteins with Cyanobacterial Photosystem I: An Integrated Computational and Experimental Model

Karan Kapoor,[†,§,∥] Derek J. Cashman,[‡,∥] Luke Nientimp,[‡] Barry D. Bruce,[*,†] and Jerome Baudry[*,†,§]

[†]Department of Biochemistry and Cellular and Molecular Biology, University of Tennessee, Knoxville, Tennessee 37996, United States

[‡]Department of Chemistry, Tennessee Technological University, Box 5055, Cookeville, Tennessee 38505-0001, United States

[§]UT/ORNL Center for Molecular Biophysics, Oak Ridge National Laboratory, Oak Ridge, Tennessee 37831, United States

Supporting Information

ABSTRACT: The stromal domain (PsaC, D, and E) of photosystem I (PSI) in cyanobacteria accepts electrons from PsaA and PsaB of photosystem I (PSI). These electrons are then used in the reduction of transiently bound ferredoxin (Fd) or flavodoxin. Experimental X-ray and NMR structures are known for all of these protein partners separately, yet to date, there is no known experimental structure of the PSI/Fd complexes in the published literature. Computational models of Fd docked with the stromal domain of cyanobacterial PSI were assembled here starting from X-ray and NMR structures of PSI and Fd. Predicted models of specific regions of protein−protein interactions were built on the basis of energetic frustration, residue conservation and evolutionary importance, as well as from experimental site-directed mutagenesis and cross-linking studies. Microsecond time-scale molecular dynamics simulations of the PSI/Fd complexes suggest, rather than a single complex structure, the possible existence of multiple transient complexes of Fd bound to PSI.

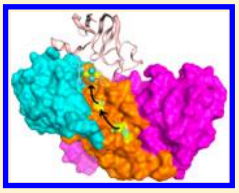

INTRODUCTION

The process of photosynthesis converts light energy into chemical energy through two large, multisubunit, pigment−protein integral membrane complexes in the thylakoid membranes of the chloroplasts of cyanobacteria, algae, and plants. These complexes are referred to as Photosystem II (PSII) and photosystem I (PSI). Upon photoexcitation, PSII extracts electrons from water, and transfers them to the cytochrome b_6/f (cyt b_6/f) complex and then reduces the PSI special pair using a soluble, one-electron-transfer protein, such as cytochrome c_6 (cyt c_6) or plastocyanin (PC). PSI then undergoes a second photoexcitation, which induces a cascade of electron transfer steps through several redox cofactors within the protein, ending up on the stromal surface after either of the two terminal electron receptors present in the PsaC chain of the stromal domain, F_A and F_B, undergoes reduction. Following this reduction, an electron is then transferred to a second mobile carrier, either ferredoxin (Fd) or flavodoxin. This transfer allows electrons to move from the membrane bound 4Fe−4S centers to ferredoxin's (Fd) 2Fe−2S center[1,2] or flavodoxin's flavin mononucleotide (FMN) cofactor under iron-deficient conditions.[3,4] The reduced Fd transfers two electrons to the ferredoxin-NADP oxidoreductase (FNR) to produce NADPH, which functions as a reducing agent in Calvin cycle reactions as well as several other metabolic processes.[5] However, due to the transient and relatively weak interaction between Fd/cyt c_6 and PSI, the molecular details of binding are not well characterized. It is crucial to elucidate the binding mechanisms and affinity of Fd and cyt c_6 with PSI to further our knowledge and understanding of the structural and functional relationships involved in the electron transfer mechanisms of photosynthesis.

The purpose of this study is to examine the atomic-level intermolecular interactions at the PSI/Fd interface from cyanobacteria using advanced computational methods integrated with experimental results. Molecular models of Fd interacting with the cyanobacterial PSI stromal domain (chains PsaC, PsaD, and PsaE) were assembled using the NMR structures of cyanobacterial Fd[6,7] and X-ray crystal structures of cyanobacterial PSI.[8] Due to the transient nature of the Fd interaction with PSI, an understanding of the large-scale domain fluctuations and movements of the protein complex is essential. In an effort to further elucidate this, docking models of PSI/Fd recently proposed by Cashman et al.[9] were subjected to microsecond time-scale molecular dynamics simulations, as well as newly generated models obtained using the ClusPro approach guided by experimental predictions of amino acid residues involved in protein−protein interactions determined by experimental site-directed mutagenesis[10,11] and cross-linking[12,13] studies. Energetically favorable models of the PSI/Fd complex are compared and ranked on the basis of the prediction of surface residues of the proteins that display a high degree of energetic "frustration" as in our previous study[9] in conjunction with predictions of the coevolving residues between the interacting partners.

Received: August 19, 2017
Revised: December 1, 2017
Published: December 6, 2017

DOI: 10.1021/acs.jpcb.7b08307
J. Phys. Chem. B 2018, 122, 1026−1036

The protein energy landscape describes the numerous different conformations that proteins may adopt during the process of folding, interaction with other proteins or nucleic acids, or binding with small molecules. This energy landscape may be described computationally using a statistical mechanical representation of the potential energy surface.[14] During the process of folding or binding, a protein adopts the state exhibiting the least amount of energetic "frustration", so there is a free energy decrease as conformations become more stable.[15] As the global conformation of folded proteins approaches this minimally frustrated state, specific regions of the protein may exhibit locally increased energetic frustration. These "frustrated" residues do not exhibit their lowest energy conformation, and it is possible that this "frustration" could be alleviated via the binding of another protein or small molecule, in the same sense that wearing a hat might alleviate the "frustration" of hairs standing straight out on a "bad hair day". The "protein frustratometer" application of energy landscape theory[15] is a computational algorithm that is capable of identifying these regions of high localized energetic frustration in protein structures.

This energy landscape based model of protein−protein interactions can be further enhanced with the addition of a complementary method of ranking amino acid residues in a protein sequence based on their evolutionary importance. The evolutionary trace method was used to determine the evolutionary importance of residues in PSI and Fd by performing a multiple sequence alignment of the proteins, and determining an importance score for highly conserved residues within the phylogenetic tree.[16,17] The residues identified with high evolutionary importance can be correlated with important functional sites in the protein, such as catalytic residues or sites of potential protein−protein interactions. The coevolutionary information obtained from evolutionary trace can be combined with the energy landscape data to yield an improved model useful in identifying sites of protein−protein interactions for further study.[18]

METHODS

Structure Preparation. Protein structures of the thermophilic cyanobacterium *Thermosynechococcus elongatus* were used to model potential interaction sites between the X-ray crystal structure of PSI and the NMR structures of Fd and PSI.[6−8] The structural files were downloaded from the PDB[19] (PDB code: 1JB0) for PSI and Fd (PDB code: 2CJN). Since the iron−sulfur center (FeS) of Fd was absent from the 2CJN NMR structure, these atoms were transferred from the 1ROE Fd NMR structure.[7] Insertion of the iron−sulfur center into 2CJN was accomplished by superimposing residues 37 through 48 of the 1ROE structure with the same residues of 2CJN, and copying the iron−sulfur center present in 1ROE to 2CJN using MOE 2015. To "smooth over" any rough contacts, conjugate gradient energy minimization was applied for 500 cycles using the AMBER99 force field in MOE 2015 to the newly modeled Fd protein. This force field was slightly modified to accommodate the calculation of atomic charges[20] and angle bending parameters for the FeS bonds,[9] which were determined from the angles observed in the 1ROE NMR structure of Fd. The protonation state of this Fd model was accomplished using estimated pK_a calculations via the Protonate3D module of MOE 2015.

Identification of Protein Surface Characteristics of PSI and Fd. The predicted possible protein−protein interaction sites between PSI's stromal domain (PsaC, D, and E) and Fd were identified using MOE 2015. Multiple residues were identified using a combination of data from site-directed mutagenesis, chemical cross-linking, and other experiments that were thought to be involved in interactions between PSI and Fd.[10,11,21,22] The relative positions of the cysteine residues surrounding Fd's iron−sulfur center[6] as well as the PsaC iron−sulfur centers, F_A and F_B, were identified in conjunction with previously published experimental residue predictions for binding sites. Clusters of amino acid residues in PSI and Fd calculated to exhibit a frustration density greater than 20% were identified using the "protein frustratometer" algorithm (EMBNet, http://www.embnet.qb.fcen.uba.ar/embnet). The evolutionary trace method (Lichtarge Computational Biology Lab, http://mammoth.bcm.tmc.edu/ETserver.html) was used to identify the residues in PSI and Fd with the highest (top 25%) importance score, and these residues were mapped out in conjunction with the frustration and biological data in MOE 2015. The residues of PSI that were used as attractive residues for subsequent ClusPro docking studies include Ile11, Thr14, Gln15, Lys34, Gly36, Val48, Lys51, and Arg52 from PsaC; His95, Asp98, Glu103, Lys104, Lys107, and Arg109 from PsaD; and Arg39 from PsaE. Two sets of docking runs were performed for comparison and to further validate the results. The first set of docking, in which the aforementioned constraints and attractive residues were used to guide the proteins toward their targets, is termed "nonagnostic" in our results. The second set of docking is termed "agnostic" in our results. The agnostic docking runs were performed without using any constraints/attractive residues in the docking protocol for comparison and validation.

Rigid-Body Docking. The fast-Fourier transform (FFT) based rigid-body docking program, ClusPro (Boston University, http://cluspro.bu.edu/),[23,24] was used for generating docking models between PSI and Fd. Two separate docking runs were carried out: first using the attractive residue constraints and the second agnostically, as discussed above. ClusPro designates one of the proteins as the "receptor" (PSI) and the other as the "ligand" (Fd). The translation and rotation of the "ligand" with respect to the "receptor" is carried out on a grid, sampling approximately 1×10^9 positions of the ligand relative to the receptor. A pairwise interaction potential scoring function is then used to score each of the translations/rotations of the ligand with respect to the receptor. Of all the generated structures, 1000 models that have the best or lowest score are clustered using pairwise Cα RMSD of "ligand" residues between different models. The goal of clustering in ClusPro is to isolate low energy minimas in the energy landscape of the complex, as these minimas are expected to be highly populated and therefore close to the native conformation sampled by the complex. After clustering, any potential adverse side chain interactions in the ranked complexes were processed by molecular mechanics energy minimization with the CHARMM[25] force field. ClusPro then outputs the centers (structures with the most neighbors) of the largest clusters.

Calculation of Fe−Fe Distances. The models generated using ClusPro were subjected to a further energy minimization of side chains (fixed backbone) to a 0.01 RMS kcal/mol/Å^2 gradient in MOE 2015, using the CHARMM27 force field.[25] For each PSI-Fd model, the original PSI structure (1JB0) was superimposed on these models to obtain the Fe_4S_4 center in PsaC. The distances were calculated between the iron atoms in corresponding Fe−S centers in PsaC and Fd.

DOI: 10.1021/acs.jpcb.7b08307
J. Phys. Chem. B 2018, 122, 1026−1036

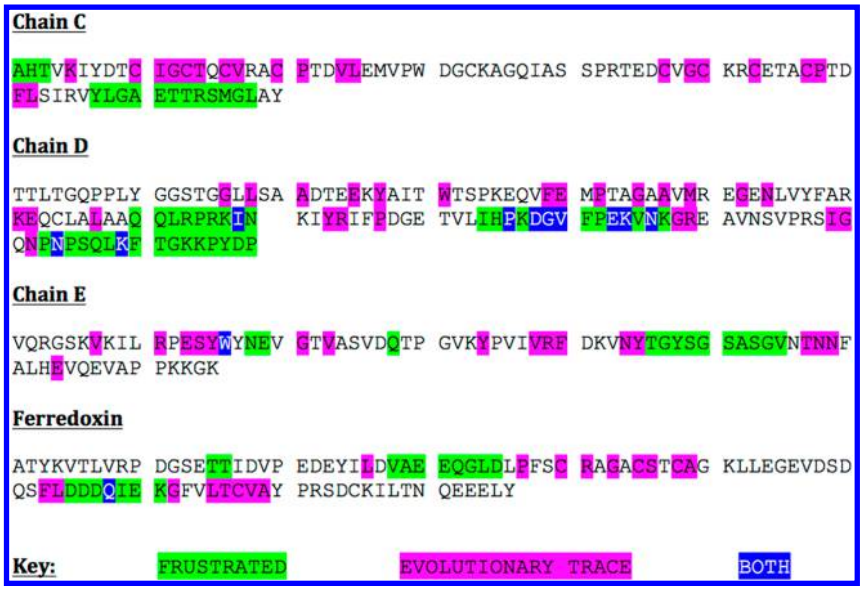

Figure 1. Primary structure of PSI-Fd (chains C, D, E, with Fd). The primary structure of PSI chains C, D, E and Fd is shown. Residues highlighted in green exhibit greater than 20% energetic frustration. Residues highlighted in magenta indicate that they have an evolutionary trace importance (rho) score in the top 25% of all residues. Residues highlighted in dark green exhibit both high (greater than 20%) evolutionary trace as well as the top 25% of importance (evolutionary trace) scores.

Molecular Dynamics Simulation of PSI/Fd Complexes. The structural dynamics of several docked complexes of PSI with Fd were investigated using all-atom molecular dynamics (MD) simulations. The starting structures for these simulations were the top three docked structural complexes of PSI/Fd previously published (model #2, #3, and #9).[9] Each protein complex was solvated using periodic boundary conditions and approximately 17,000 TIP3P water molecules.[33,34] Molecular dynamics simulation was accomplished using NAMD2 version 2.9 and the AMBER99 all-atom force field, as implemented in MOE 2015, at a simulation temperature of 300 K. The AMBER99 force field was modified to include the angle bending and torsional parameters for the FeS bonds present in PSI and Fd as previously described (Supporting Information, Table S1). The integration step used was 2 fs, and all of the hydrogen atomic distances in the system were set to equilibrium values. Each of the systems that were simulated underwent initial conjugate gradient energy minimization for 2000 steps. Next, each system was progressively heated incrementally using an equilibration procedure from 100 to 300 K. Each increment was 50 K for 100 ps, until equilibrium temperature was reached at 300 K. The production run for each system was 1 μs. Since the stromal domain of PSI is membrane-bound, the backbone atoms of the residues observed to be in contact with PsaA, PsaB, and PsaF of PSI were fixed, while the side chains were allowed full range of movement during the simulations (Supporting Information, Figure S1). The simulations were completed on the Hopper supercomputing cluster at Lawrence Berkeley National Laboratory through a grant received through the NERSC program (U.S. Department of Energy Office of Science Contract No. DE-AC02-05CH11231).

RESULTS

Identification of Protein Surface Characteristics of PSI and Fd. The energetic frustration and evolutionary trace data together suggest a good model for possible docking sites of Fd with PSI (Figure 1, Figure 2, Figure 3). As a general

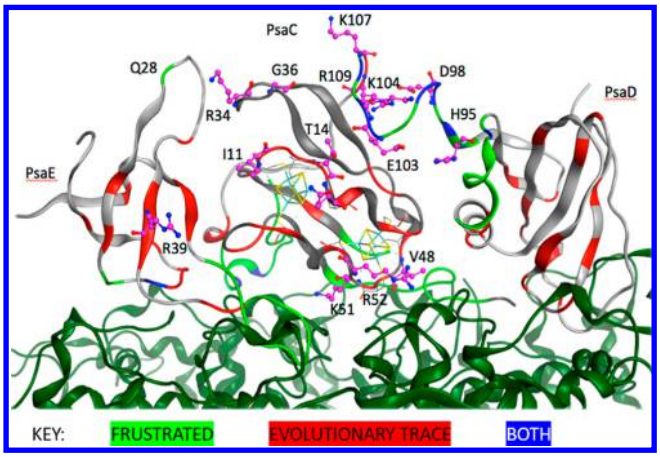

Figure 2. PSI stromal domain model indicating residues of interest. The key residues that may play a role in Fd binding are highlighted in this view of the stromal domain of PSI. Residues highlighted with green ribbons exhibit greater than 20% energetic frustration. Residues highlighted with red ribbons indicate that they have an evolutionary trace importance (rho) score in the top 25% of all residues. Residues highlighted with dark blue ribbons exhibit both high (greater than 20%) evolutionary trace as well as the top 25% of importance (evolutionary trace) scores.

observation, regions of favorable evolutionary importance do not appear to be highly energetically frustrated. Furthermore, as expected, all of the cysteine residues that are directly linked to one of the iron−sulfur centers in both PSI and Fd were calculated by evolutionary trace to be of critical importance with a favorable evolutionary trace score, indicating a high degree of conservation and biological importance.[16,17] Of particular interest are several residues in PsaE, centered around Arg-39. Previously published backscattering interferometry data suggests that Arg-39 might be important to binding Fd.[10] The evolutionary trace and energetic frustration data suggests some additional residues in the stromal domain that may contribute to the binding between PSI and Fd. These residues are

DOI: 10.1021/acs.jpcb.7b08307
J. Phys. Chem. B 2018, 122, 1026−1036

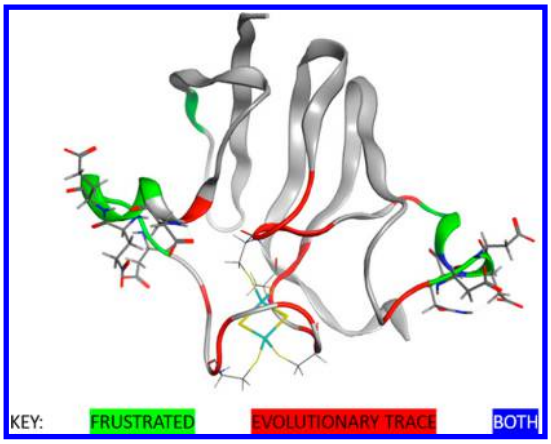

Figure 3. Ferredoxin model indicating residues of interest. The key residues of Fd that may play a role in binding with PSI are highlighted in this view. Residues highlighted with green ribbons exhibit greater than 20% energetic frustration. Residues highlighted with red ribbons indicate that they have an evolutionary trace importance (rho) score in the top 25% of all residues. Residues highlighted with dark blue ribbons exhibit both high (greater than 20%) evolutionary trace as well as the top 25% of importance (evolutionary trace) scores.

concentrated around two discrete regions of PsaE—between Arg-11 and Glu-19 and Gln-28 and Tyr-45.

PSI-Fd Modeling. PSI-Fd models generated using attractive residue constraints in ClusPro consisted of a total of 12 separate clusters represented by their cluster centers. Each of these cluster centers from ClusPro is labeled "CC1" through "CC12" in the data. For comparison, the previously published docking data from Cashman et al.[9] is labeled "1" through "12". Table 1 shows these 12 clusters, the number of members belonging to each cluster, and the weighted energy scores. Figure 4A shows the Cα RMSD between these 12 clusters calculated in MOE 2015. These 12 structures are separated by large RMSD distances, with the closest centers (CC7 and CC10) showing a RMSD deviation of 3.71 Å. These 12 structures can be considered as separate PSI-Fd states that are possibly sampled, weighted against the cluster population represented by each cluster center; i.e., cluster 1 center (CC1) represents the structure most sampled and hence closest to the native state of the complex.

Table 2 shows the number of inter-residue protein contacts and the Fe−Fe distances between the FeS centers in PsaC and Fd in each of these 12 cluster centers. The top three models (cluster centers with largest populations) identified more inter-residue contacts compared to previously published rigid body directed docking models of PSI-Fd.[9] The Fe−Fe distances on average are also closer than the previously published models, with the lowest distance shown by the third model (8.5 Å). The average Fe−Fe distances were 8.9−13.1 Å between each of the two FeS centers (F_A and F_B) of PsaC. Distances similar to these were previously observed in six PSI crystal structures: *T. elongatus*, *Pisum sativum*, and *Arabidopsis thaliana*.[8,26−29] The fact that the generated models yield similar Fe−Fe distances to that observed in the crystal structures between F_A and F_B suggests that these docked models would be close enough to permit rapid electron transfer.[30] Superposition of these 12 cluster centers shows Fd sampling multiple rotational modes around the same binding site near the PSI FeS center, shown in Figure 5A.

Table 1. PSI-Fd Models Generated Using ClusPro[a]

cluster	members	representative	weighted score
CC1	247	center	−744
CC1	247	lowest energy	−852
CC2	163	center	−712.6
CC2	163	lowest energy	−850.2
CC3	140	center	−714.4
CC3	140	lowest energy	−815.2
CC4	119	center	−723.2
CC4	119	lowest energy	−882.8
CC5	106	center	−712.4
CC5	106	lowest energy	−870.7
CC6	53	center	−729.7
CC6	53	lowest energy	−784.2
CC7	44	center	−740.2
CC7	44	lowest energy	−808.2
CC8	38	center	−723
CC8	38	lowest energy	−769.5
CC9	22	center	−747.9
CC9	22	lowest energy	−805.5
CC10	18	center	−720.5
CC10	18	lowest energy	−758
CC11	13	center	−754.3
CC11	13	lowest energy	−754.3
CC12	6	center	−706.3
CC12	6	lowest energy	−753.4

[a]The 12 cluster centers, labeled CC1 through CC12, showing the number of members belonging to each cluster, and the weighted energy scores.

The "agnostic docking" protocol in ClusPro generated a total of 18 cluster centers, shown in Table 3. Superposition of these 18 cluster centers with the 12 models generated with the nonagnostic approach is shown in Figure 5B. Twelve of the 18 models generated using the agnostic approach bind to the same binding surface formed between the three subunits of PSI sampled by the 12 models generated by the nonagnostic approach. In the remaining six models, showing relatively low cluster populations, Fd binds to the opposite side of PSI. This lumenal surface of PSI revealed PSI residues on PsaA, PsaB, and PsaF of PSI that could provide favorable binding of Fd in a detergent solubilized solution form of PSI, yet due to the topology of PSI in the membrane, this interaction would be prohibited *in vivo*. As expected, this binding region is not sampled in the nonagnostic approach due to the constraints placed on the system.

Figure 5C shows the superposition of the two top models generated using the nonagnostic and agnostic docking protocols, respectively. These two models are similar to each other with a Cα RMSD of 1.70 Å between the structures. The small RMSD is present likely due to the differences generated in the energy minimization step carried out after the model generation in ClusPro. The models show direct interactions between Arg-41, Ser-63, Glu-23, and Glu-93 in Fd and the residues in PsaC, PsaD, and PsaE that have been shown to be important for binding Fd through mutagenesis studies (Gln-15 in PsaC, Lys-34 in PsaC, Lys-104 in PsaD, and Arg-39 in PsaE, respectively), given in Table 4. This complex structure, the distance between the FeS centers, and two salt bridges between Arg-39 in PsaE and Lys-104 in PsaD and Glu-93 and Glu-23 in Fd, respectively, are shown in Figure 5D. Lys-34 of PsaC is positioned near the interface between PsaC and PsaE. Previous

DOI: 10.1021/acs.jpcb.7b08307
J. Phys. Chem. B 2018, 122, 1026−1036

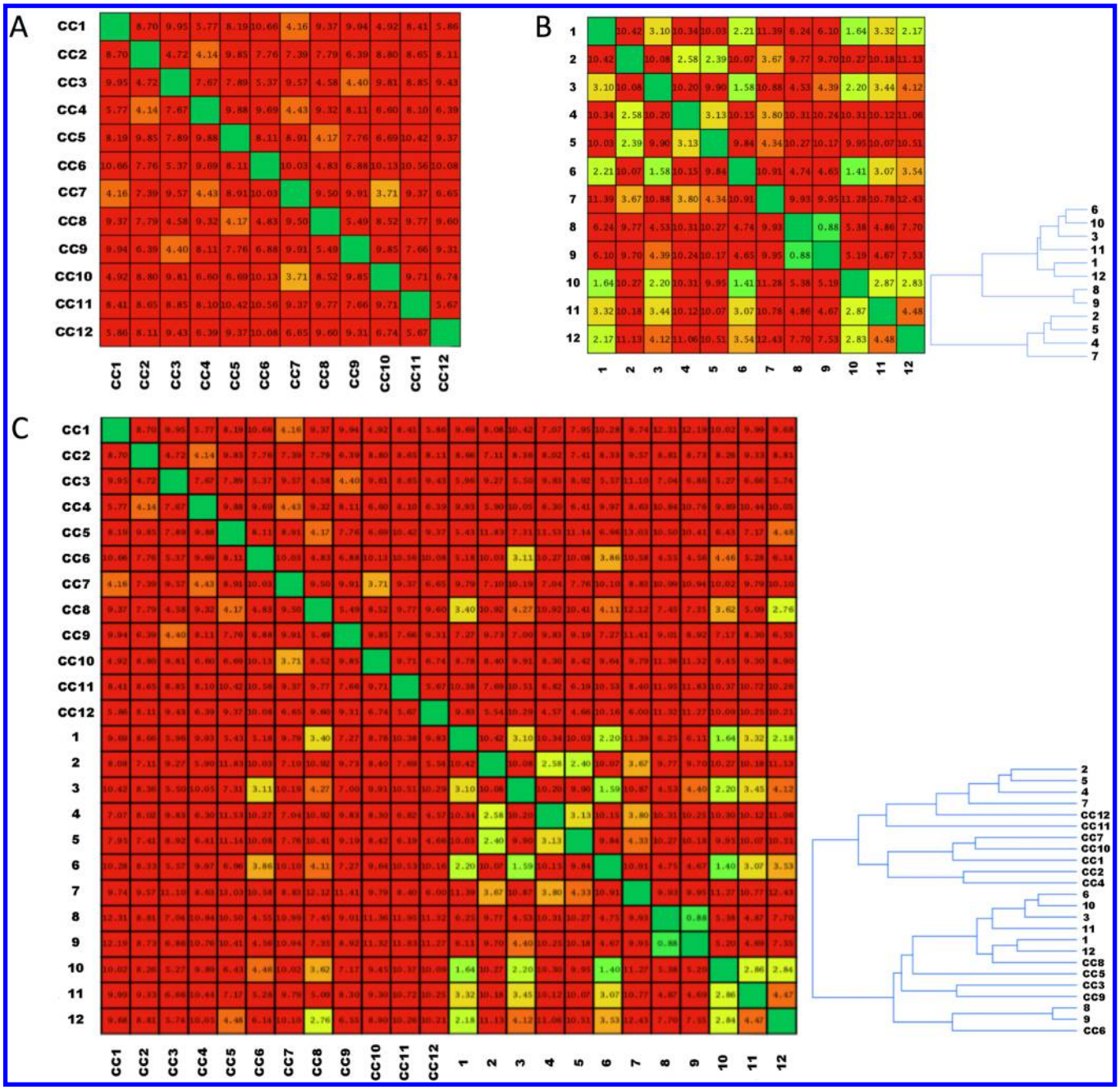

Figure 4. (A) PSI-Fd models generated using ClusPro. RMSD deviation between 12 cluster center from the nonagnostic (attractive residue constrain) approach. RMSD deviation from each cluster center is labeled with "CC1" through "CC12". The color of each square indicates the average RMSD of each compex: dark green, RMSD = 0; yellow/bright green, RMSD < 3; orange, RMSD 3−5; red, RMSD > 5. (B) Comparison with previously published PSI-Fd models. RMSD deviation between previously published 12 models of PSI-Fd represented by three clusters. This data from the previously published models (Cashman et al.[9]) is labeled 1 through 12. The color of each square indicates the average RMSD of each compex: dark green, RMSD = 0; yellow/bright green, RMSD < 3; orange, RMSD 3−5; red, RMSD > 5. (C) Comparison with previously published PSI-Fd models. Comparison of RMSD of the newly generated models to the previous models. RMSD deviation from each cluster center of the ClusPro models is labeled with "CC1" through "CC12". RMSD deviation from the previously published models (Cashman et al.[9]) is labeled 1 through 12. The color of each square indicates the average RMSD of each compex: dark green, RMSD = 0; yellow/bright green, RMSD < 3; orange, RMSD 3−5; red, RMSD > 5.

experimental mutations of the analogous Lys-35 residue in *C. reinhardtii* by Fischer and co-workers indicate that this residue is critically important for binding of Fd to PsaD and PsaE as well as electron transfer reactions.[31] In our model, the Lys-34 residue is involved with a strong salt bridge interaction with Asp-27 of PsaE and is involved, along with the Lys-33 residue of PsaE, in forming salt bridge interactions at the PsaC/PsaE interface holding the entire protein together. Disruption of any of these interactions will contribute to instability in the stromal domain trimer, resulting in loss of electron transfer capabilities.

The previously published models of PSI-Fd consisted of a set of 12 models (9) represented by only three clusters shown in Figure 4B: cluster I represented by structures 2, 4, 5, and 7; cluster II represented by structures 1, 3, 6, 10, 11, and 12;

DOI: 10.1021/acs.jpcb.7b08307
J. Phys. Chem. B 2018, 122, 1026−1036

Table 2. PSI-Fd Model Contacts and Fe−Fe Distances[a]

models	inter-residue protein contacts	Fe−Fe distance (Å)
CC1	29	11.7
CC2	24	9.9
CC3	25	8.5
CC4	26	9.7
CC5	23	13.5
CC6	27	9.95
CC7	27	12.4
CC8	22	10.8
CC9	33	15.7
CC10	25	12.6
CC11	25	21.6
CC12	29	12.4

[a]The number of inter-residue protein contacts and the Fe−Fe distances between the FeS centers in PsaC and Fd in each of the 12 cluster centers.

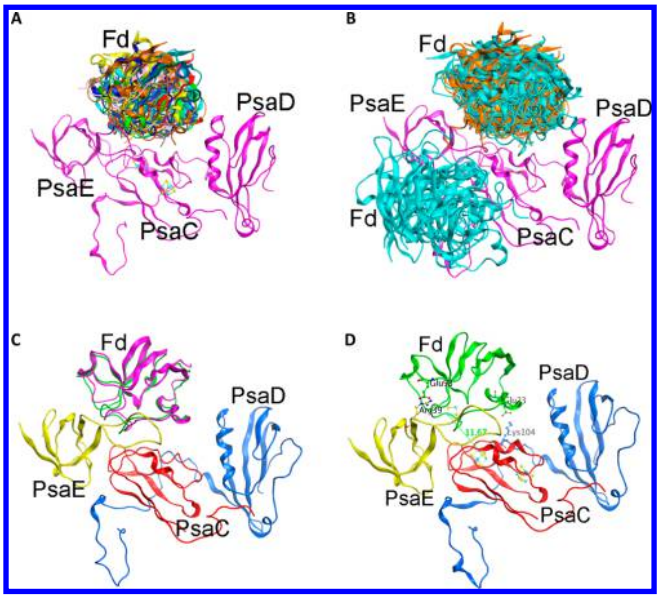

Figure 5. PSI-Fd models generated using ClusPro. (A) Superposition of these 12 cluster centers. (B) Superposition of 12 cluster centers (orange) from the nonagnostic approach and 18 models (cyan) from the agnostic approach. (C) Superposition of two top models using the nonagnostic, Fd in green, and agnostic docking protocols, Fd in purple. (D) Distance between FeS centers and salt bridges between PSI and Fd in the top model from the nonagnostic approach.

cluster III represented by structures 8 and 9. These 12 structures are separated by relatively short RMSD distances. Figure 4C shows the comparison of the RMSD of the newly generated models to the previous models. Structures in cluster I are found to be similar to the CC12 model; cluster II structures are similar to the CC8 model; and cluster III structures are similar to the CC6 model, with the orientation exhibiting the most favorable potential interaction energy (3 in Figure 4B) from the previous models predicted to be structurally close to the eighth model (CC8 in Figure 4A) predicted by ClusPro. The previous three clusters (consisting of 12 models) likely represent a subset of the conformational ensemble sampled by PSI-Fd, as seen from the much larger ensemble of structures generated by ClusPro, both by nonagnostic and agnostic approaches.

Table 3. PSI-Fd Models Generated Using ClusPro Using Agnostic Docking[a]

cluster	members	representative	weighted score
1	248	center	−615.7
1	248	lowest energy	−698.8
2	99	center	−597.5
2	99	lowest energy	−667.4
3	85	center	−590.8
3	85	lowest energy	−685.6
4	79	center	−592.9
4	79	lowest energy	−648.6
5	77	center	−590.6
5	77	lowest energy	−728.1
6	64	center	−595.3
6	64	lowest energy	−711.5
7	57	center	−607.1
7	57	lowest energy	−690.5
8	51	center	−622
8	51	lowest energy	−650.9
9	43	center	−685.4
9	43	lowest energy	−685.4
10	39	center	−589
10	39	lowest energy	−646
11	32	center	−626.9
11	32	lowest energy	−676.7
12	28	center	−603.9
12	28	lowest energy	−636
13	17	center	−583.1
13	17	lowest energy	−632.8
14	16	center	−585.1
14	16	lowest energy	−647.8
15	14	center	−592.6
15	14	lowest energy	−614.9
16	14	center	−595.4
16	14	lowest energy	−684.1
17	4	center	−585.8
17	4	lowest energy	−628.2
18	4	center	−596.8
18	4	lowest energy	−604.7

[a]The 18 clusters, the number of members belonging to each cluster, and the weighted energy scores.

Molecular Dynamics Simulation of PSI/Fd Complexes.

Extended molecular dynamics simulations of 1 μs in duration were run using NAMD on the three most favorable complexes from each major cluster generated by the Cashman et al. study.[9] Figure 6 shows the root-mean-square deviation (RMSD) versus time for the full 1 μs molecular dynamics trajectory of each of the three simulated PSI-Fd complexes. Two of the simulations exhibited equilibration of the molecular dynamics trajectory at approximately 4 Å (model 3) and 6 Å (model 9), respectively. The simulation for the model 2 trajectory initially showed a rough equilibration at approximately 5 Å, followed by a major conformational change after approximately 700 ns, followed by a subsequent equilibration and repositioning with a distance of ∼8 Å. This was due to a complete reorientation of Fd in the stromal domain. Although the significance of this rearrangement is not known, it is still close enough to enable electron transfer.

A comparison of the average RMSD calculated for each respective subunit of PSI and Fd provides some information regarding the movement of the individual residues of the

DOI: 10.1021/acs.jpcb.7b08307
J. Phys. Chem. B 2018, 122, 1026−1036

Table 4. PSI-Fd Best Model Interactions[a]

type	chain	position	residue/atom	chain	position	residue
HB	PsaC	13	CYS13.O	Fd	41	ARG41.NE
HB	PsaC	15	GLN15.OE1	Fd	41	ARG41.NE
HB	PsaC	18	ARG18.NH1	Fd	23	GLU23.OE1
HB	PsaC	18	ARG18.NE	Fd	30	GLU30.OE2
HB	PsaC	18	ARG18.NH2	Fd	31	GLU31.OE1
HB	PsaC	34	LYS34.NZ	Fd	63	SER63.OG
HB	PsaD	73	ARG73.NH1	Fd	31	GLU31.OE1
HB	PsaD	76	LYS76.NZ	Fd	22	ASP22.OD2
HB	PsaD	104	LYS104.NZ	Fd	23	GLU23.OE2
HB	PsaE	3	ARG3.NH1	Fd	66	ASP66.OD1
HB	PsaE	3	ARG3.NH2	Fd	68	ASP68.OD1
HB	PsaE	25	SER25.OG	Fd	44	ALA44.O
HB	PsaE	39	ARG39.NH1	Fd	46	SER46.O
HB	PsaE	39	ARG39.NH2	Fd	93	GLU93.OE2
HB	PsaE	48	TYR48.N	Fd	35	ASP35.OD2
HB	PsaE	51	SER51.OG	Fd	35	ASP35.OD2
HB	PsaE	53	SER53.OG	Fd	11	ASP11.OD1
HB	PsaE	57	THR57.O	Fd	39	SER39.OG
HB	PsaE	57	THR57.OG1	Fd	47	THR47.OG1
ION	PsaC	18	ARG18.NH1	Fd	23	GLU23.OE1
ION	PsaC	18	ARG18.NH1	Fd	27	ASP27.OD2
ION	PsaC	18	ARG18.NE	Fd	30	GLU30.OE2
ION	PsaC	18	ARG18.NH2	Fd	31	GLU31.OE1
ION	PsaD	73	ARG73.NH1	Fd	31	GLU31.OE1
ION	PsaD	76	LYS76.NZ	Fd	22	ASP22.OD2
ION	PsaD	104	LYS104.NZ	Fd	23	GLU23.OE2
ION	PsaE	3	ARG3.NH1	Fd	66	ASP66.OD1
ION	PsaE	3	ARG3.NH2	Fd	68	ASP68.OD1
ION	PsaE	39	ARG39.NH2	Fd	93	GLU93.OE2

[a]Interactions between PSI and Fd in the top model (cluster center with largest cluster populations).

various subunits relative to other atoms in each subunit. For example, in the model 3 trajectory, the average RMSD of PsaC is 3.3 Å, the average RMSD of PsaD is 2.4 Å, the average RMSD of PsaE is 2.2 Å, and the average RMSD of Fd is 3.2 Å. For the model 9 trajectory, the average RMSD of PsaC is 2.8 Å, the average RMSD of PsaD is 1.9 Å, the average RMSD of PsaE is 1.0 Å, and the average RMSD of Fd is 2.6 Å. This data clearly indicates that there are more fluctuations among residues of PsaC and Fd than among residues of PsaD and PsaE.

The root-mean-square fluctuations (RMSF) also provides evidence of substantial movement among residues in PsaC and ferredoxin (Figure 7). The specific residues in Fd that show the greatest fluctuations are the aspartate and glutamate residues at the ends of the protein, on either side of the Fe_2-S_2 site. The cysteine residues immediately adjacent to this site also exhibit high RMSF activity as well. In PsaC, there is also significant fluctuation in the residue chain surrounding the two Fe_4-S_4 sites as well. These surface residues in PsaC correlate closely with previous electron microscopy and image analysis of the flavodoxin binding site presented by Muhlenhoff and colleagues.[3] The increased fluctuations in surface residues at the interface regions of both PsaC and Fd correlate well with previous laser flash absorption spectroscopy observations by Setif and co-workers, indicating that there are two distinct first order interactions involved in the interaction of Fd with PSI.[32] The two electron transfer rates previously observed most likely represent different binding conformations between the two species, which would likely be caused by different fluctuations in the surface residues at the binding site.[32]

Of particular interest in the interactions between PSI and Fd is the question of whether the iron−sulfur clusters of these proteins reach electron transfer capable distances. A seminal paper by Moser and colleagues suggests that most biological electron transfer in or between proteins occurs when electron transfer distances are 14 Å or less.[33] To determine if our models comply with this rule, we tracked the closest distance between atoms between the two Fe_4-S_4 complexes, F_A/F_B, present in PsaC (Figure 8), and the closest distance between atoms of the Fe_4-S_4 iron sulfur complex, F_B, and the Fe_2-S_2 complex of Fd (Figure 9). This data shows that electron transfer is clearly possible between both F_A/F_B iron−sulfur complexes present in PsaC, as well as two of the docked conformations (model 3 and model 2) between F_{Fd}/F_B, the F_B iron−sulfur complex of Fd, and the iron−sulfur of PSI. Overall, these electron transfer distances between the F_{Fd}/F_B iron−sulfur complexes compare very favorably to the electron transfer distances done by ClusPro docking. We also observe a major molecular movement in the model 2 simulation that reveals a significant conformational repositioning of Fd on the stromal domain of PSI after ∼700 ns; this movement reduces the F_{Fd}/F_B iron−sulfur distances from a high of 17 Å to a low of about 13 Å.

DISCUSSION AND CONCLUSION

The ClusPro rigid body docking calculations in conjunction with extended microsecond molecular dynamics provide some key insights into the transient nature of the PSI/Fd interaction. While the ClusPro data illustrates a comprehensive look into

DOI: 10.1021/acs.jpcb.7b08307
J. Phys. Chem. B 2018, 122, 1026−1036

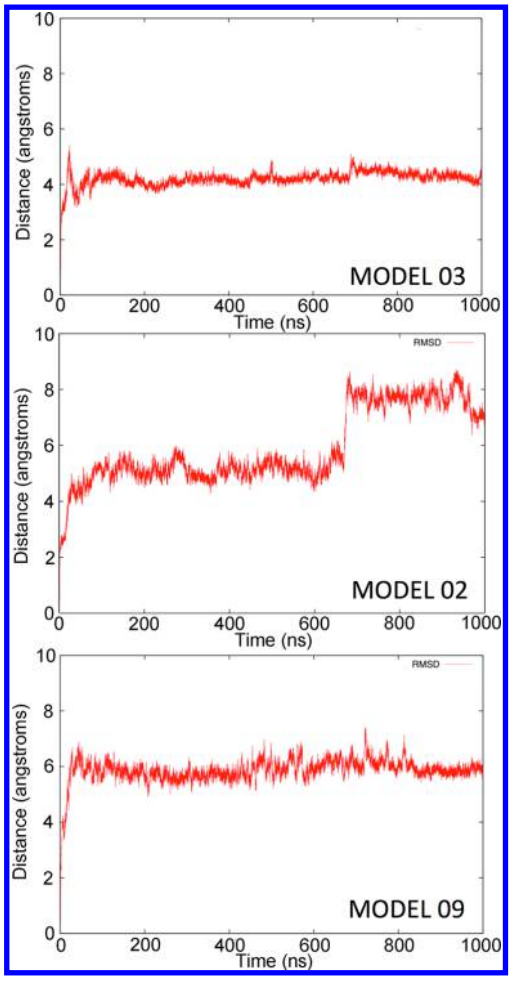

Figure 6. RMSD vs time of simulated PSI-Fd complexes. The root-mean-square deviation of each protein complex over the course of the 1 μs simulation shows the relative fluctuations over time.

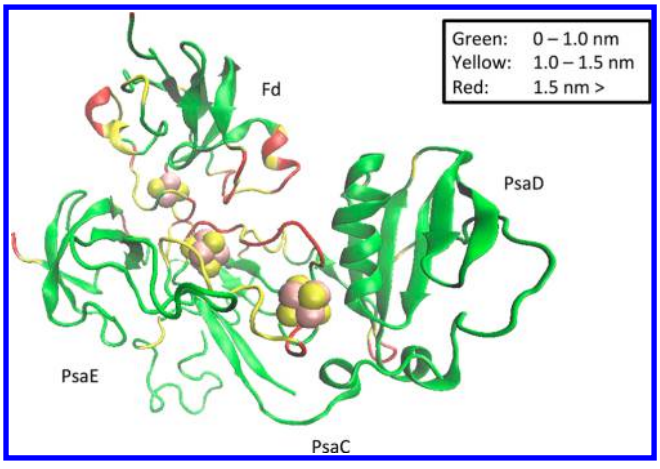

Figure 7. Root-mean-square fluctuations (RMSF) of all residues of the model 3 simulation trajectory. RMSF data for the 1 μs model 3 trajectory shows specific parts of the protein complex that are undergoing more movements and fluctuations.

the complete energy landscape of possible docked conformations, the molecular dynamics simulations identify specific parts of the catalytic site of each protein exhibiting high fluctuations, and show how catalytically inactive electron transfer con-

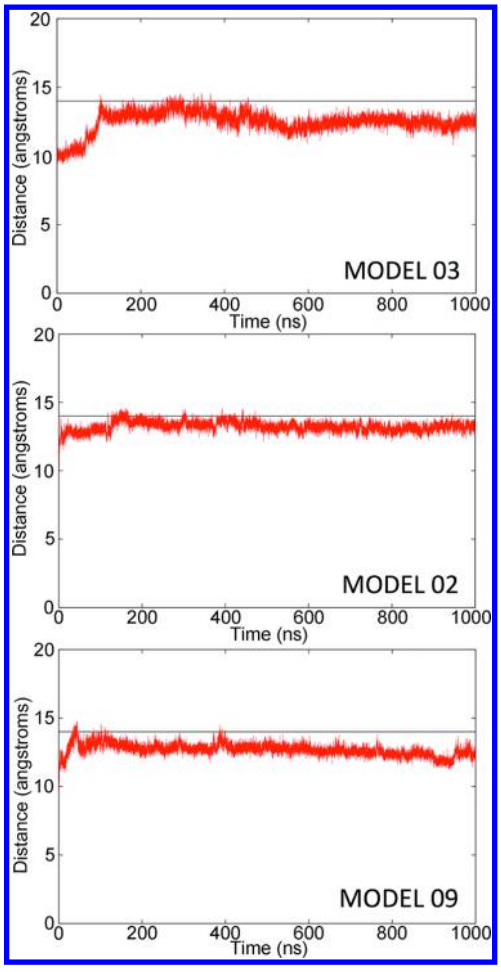

Figure 8. Distances in angstroms (Å) throughout the 1000 ns trajectory between the closest atoms of the F_A/F_B iron–sulfur complexes in PsaC. The distance between the two iron–sulfur complexes in PsaC is shown to indicate how far an electron would need to travel to be transferred between each complex. The horizontal black line drawn at 14 Å represents the cutoff in maximum electron transfer distance in the Moser et al. paper.[33]

formations can transition to catalytically active electron transfer conformations.

The ClusPro rigid body docking calculations yield several observations with regard to possible interactions between the electron-transport protein, Fd and PSI. Docking calculations focused on the stromal (PsaC, PsaD, PsaE) domain of PSI where these electron-transport proteins bind. Previously published PSI-Fd models[9] had used a "top-down" approach by using the regions of high frustration to direct manual rigid-body docking calculations using MOE 2015, with distance constraints applied between the possibly interacting residues/regions. In the ClusPro docking study, only the residues in PSI that have been shown to interact with the electron-transport proteins have been used to influence the docking calculations. This allows the receptor and the ligand in the rigid-body docking protocol to adequately sample all six degrees of freedom, generating ~10^9 positions of the ligand relative to the receptor. These are then filtered to only keep the structures that are thermodynamically most stable, giving preference to the complexes that show interactions between the input residues. This provides a "bottoms-up" approach, where the best models are predicted from the possible ~10^9 generated

DOI: 10.1021/acs.jpcb.7b08307
J. Phys. Chem. B 2018, 122, 1026–1036

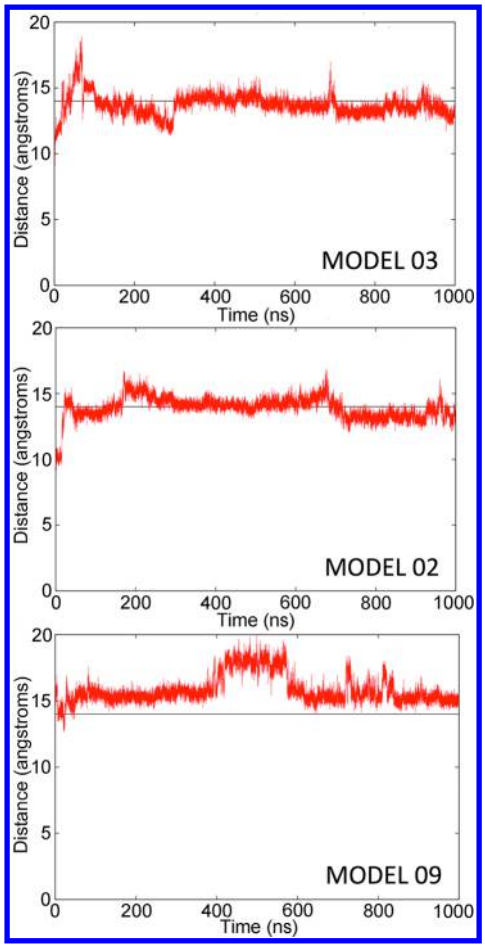

Figure 9. Distances in angstroms (Å) throughout the 1000 ns trajectory between the closest atoms of the F_{Fd}/F_B iron−sulfur complexes in PsaC. The distance between the iron−sulfur complexes in PsaC (F_B) and the iron−sulfur complex in Fd (F_{Fd}) is shown to indicate how far an electron would need to travel to be transferred from PSI to Fd. The horizontal black line drawn at 14 Å represents the cutoff in maximum electron transfer distance in the Moser et al. paper.[33]

models, hence decreasing the possibility of sampling only certain fixed rotational/translational modes of the ligand with respect to the receptor.

The top cluster center for the PSI-Fd model shows direct interactions between the residues experimentally predicted to be important for binding Fd, Gln-15 in PsaC, Lys-34 in PsaC, Lys-104 in PsaD, and Arg-39 in PsaE, and the Arg-41, Ser-63, Glu-23, and Glu-93 residues of Fd. There are two salt bridges present between Arg-39 in PsaE and Glu-93 in Fd, and Lys-104 in PsaD and Glu-23 in Fd. Low RMSD between the top PSI-Fd models (Figure 4C) generated using the nonagnostic and agnostic docking protocols highlights the preference for the top binding mode generated by using two separate approaches.

The previous PSI-Fd rigid body directed docking models can be represented by a subset of the newly generated models. Hence, the new results provide a more comprehensive picture of the possible binding modes. Fd is found to sample multiple rotational modes around the same binding site near the PSI Fe_4-S_4 center. Furthermore, simulation of the top three previous PSI-Fd rigid body directed docking models indicates that Fd does indeed sample multiple rotational modes around the same binding site through the course of a 1 μs trajectory. Several residue contacts involving salt bridges and hydrogen bonding also exhibited significant fluctuations through the course of the simulations. For example, in the simulation of the PSI-Fd rigid body directed docking model 3, the PsaE Arg-3 and Fd Glu-30 residues started at 6.7 Å, went to a high of approximately 26.8 Å, and equilibrated at the end at 2.8 Å. Other residue pairs between the stromal domain and Fd also exhibited similarly wide fluctuations, always equilibrating at the end of the simulation within about 3 Å of each other. These residue pairs include, for the model 3 interaction, PsaC Gln-15 and Fd Asp-66, PsaC Arg-18 and Fd Asp-66, PsaD Lys-104 and Fd Glu-71, PsaD Lys-107 and Fd Tyr-97, and PsaE Arg-3 and Fd Glu-30. These models show that the electrostatic interactions of all three subunits of the stromal domain—PsaC, PsaD, and PsaE—are critically important in bonding with Fd for electron transfer to occur. While the direct contact between PsaC and Fd is at the physical center of electron transfer, PsaD and PsaE play a role in the positioning of Fd to enable the transfer of electrons to take place. The trimeric complex is analogous to a baseball glove when catching a ball—as a fast-moving ball (protein) makes contact with parts of the glove (residues of PsaC, PsaD, and PsaE), the ball is positioned better in the glove. Just as a baseball may have more than one conformation in the glove, Fd may adopt more than one electron-capable conformation in the stromal domain of PSI. Minor changes to one or two of these critical residues of PsaD and PsaE may be able to be tolerated, but if too many residues are changed significantly, this would lead to loss in the ability of the PSI complex to form stable electron transfer interactions.

Both of the ClusPro docking results as well as the microsecond molecular dynamics simulations suggest that there is more than one favorable docking conformation capable of electron transfer of Fd with PSI. This is based on analysis of the F_{Fd}/F_B distances between iron−sulfur clusters between both proteins, as shown in Table 2 for the ClusPro docking data, the root-mean-square fluctuations (RMSF) in Figure 7, and Figure 9 for the molecular dynamics simulation trajectories. The presence of two distinct modes of binding between Fd and PSI has also been observed experimentally by Setif and colleagues using laser flash absorption spectroscopy.[32] This is significant biologically due to the extremely short time scale involved in biological electron transfer—if more than one binding mode allows electron transfer, less time is necessary, ensuring that proteins are docked in their correct position and reduction can occur at a fast rate. All but two of the cluster centers from the ClusPro docking calculations suggest an electron transfer distance below the 14 Å threshold for biological electron transfer, and two out of the three simulations performed show electron transfer distances below 14 Å as well.[33] Previous Brownian dynamics simulations and experimental studies of cytochrome c (Fe^{3+})−cytochrome b_5 (Fe^{2+}) suggest that electron transfer in proteins is possible in an ensemble of multiple docked conformations as opposed to a single, static structure.[34−36]

Furthermore, the energetic frustration and evolutionary trace analysis of the proteins of PSI and Fd are particularly effective at predicting the residues involved at the interface in both the previous PSI-Fd rigid body directed docking models, the ClusPro docking models, as well as residues observed at the interface in the simulations of the rigid body directed docking models. While the energetic frustration model alone is sufficient to serve as a guide for a thorough ClusPro docking study between two proteins, the addition of the evolutionary trace

DOI: 10.1021/acs.jpcb.7b08307
J. Phys. Chem. B 2018, 122, 1026−1036

model provides another dimension in this analysis and yields complementary information about amino acid residues of high importance at the docking interface.

While this research focuses on trimeric PSI formation, it is known that a small pool of monomeric PSI subunits is known to exist, influenced by intracellular Ca^{2+} levels as well as the amount of light.[37] Trimerization of PSI is mediated by the transmembrane chains, PsaL, PsaI, and PsaM. In mutant strains of *Synechocystis sp. PCC 6803* that lack PsaL, and hence do not form trimers, Fd binds and photosynthesis has been shown to continue.[37] An interesting topic of future study might be to perform docking and molecular dynamics simulations of monomeric PSI and Fd and observe the possible different conformations present. Without the addition of the extra two domains to assist in stabilizing the conformational possibilities, one might expect to observe an increased number of electron transfer capable docked conformations of Fd docked with monomeric PsaC.

Overall, this study illustrates new and detailed insights into understanding the initial binding mechanisms between PSI and Fd. These complexes are involved in the electron transfer reactions of photosynthesis, and a thorough understanding of their atomic-level interactions and dynamics will help in suggesting future mutagenesis experiments for validation purposes. These will also enable in the design more of efficient mutants of these proteins, to optimize the rate of electron transfer and hence the rate of energy generation from these systems, leading to the development of biologically based solar energy cells for electricity generation.

■ ASSOCIATED CONTENT

Supporting Information

The Supporting Information is available free of charge on the ACS Publications website at DOI: 10.1021/acs.jpcb.7b08307.

AMBER99 force field angle bending parameters used for the FeS complexes in molecular models; description of backbone atoms of residues in contact with the membrane-bound region of PSI in which the backbone atoms are fixed during simulations (PDF)

Special Issue Paper

This paper was originally submitted for the http://pubs.acs.org/toc/jpcbfk/121/15?ref=jpcbfkFeature "Klaus Schulten Memorial Issue", published as the April 20, 2017, issue of *J. Phys. Chem. B* (Vol. 121, No. 15).

■ AUTHOR INFORMATION

Corresponding Authors

*Address: 226 Hesler Biology, 1414 Cumberland Ave., Knoxville, TN 37996. Phone: (865) 974-4082. Fax: (865) 974-6306. E-mail: bbruce@utk.edu.

*Address: University of Alabama in Huntsville, Department of Biological Sciences. E-mail: jerome.baudry@uah.edu.

ORCID

Karan Kapoor: 0000-0002-7719-0274

Jerome Baudry: 0000-0002-1969-1679

Author Contributions

‖K.K., D.J.C.: These authors contributed equally to the work.

Notes

The authors declare no competing financial interest.

■ ACKNOWLEDGMENTS

This work is dedicated to the memory of Klaus J. Schulten, in admiration and in gratitude for his work and for his leadership. This work has been made possible by the simulation and visualization programs he and his co-workers have developed over the years, and by the inspiration he gave to the entire field of computational molecular biophysics. This research was funded by a subcontract awarded to D.J.C. and J.B. of the Tennessee Solar Conversion and Storage Using Outreach, Research & Education (TN-SCORE) from grant of the National Science Foundation to the University of Tennessee at Knoxville (EPS-1004083) to B.D.B. This research used resources of the National Energy Research Scientific Computing Center, a DOE Office of Science User Facility supported by the Office of Science of the U.S. Department of Energy under Contract No. DE-AC02-05CH11231.

■ REFERENCES

(1) Zanetti, G.; Merati, G. Interaction Between Photosystem-I and Ferredoxin: Identification by Chemical Cross-Linking of the Polypeptide Which Binds Ferredoxin. *Eur. J. Biochem.* **1987**, *169* (1), 143−146.

(2) Zilber, A. L.; Malkin, R. Ferredoxin Cross-Links to a 22 kD Subunit of Photosystem I. *Plant Physiol.* **1988**, *88* (3), 810−4.

(3) Muhlenhoff, U.; Kruip, J.; Bryant, D. A.; Rogner, M.; Setif, P.; Boekema, E. Characterization of a Redox-Active Cross-Linked Complex Between Cyanobacterial Photosystem I and its Physiological Acceptor Flavodoxin. *EMBO J.* **1996**, *15* (3), 488−497.

(4) Setif, P. Ferredoxin and Flavodoxin Reduction by Photosystem I. *Biochim. Biophys. Acta, Bioenerg.* **2001**, *1507* (1−3), 161−179.

(5) Berg, J. M.; Tymoczko, J. L.; Stryer, L. *Biochemistry*, 6th ed.; W.H. Freeman & Company: New York, 2007.

(6) Hatanaka, H.; Tanimura, R.; Katoh, S.; Inagaki, F. Solution Structure of Ferredoxin From the Thermophilic Cyanobacterium Synechococcus Elongatus and its Thermostability. *J. Mol. Biol.* **1997**, *268* (5), 922−33.

(7) Baumann, B.; Sticht, H.; Scharpf, M.; Sutter, M.; Haehnel, W.; Rosch, P. Structure of Synechococcus Elongatus [Fe2S2] Ferredoxin in Solution. *Biochemistry* **1996**, *35* (39), 12831−41.

(8) Jordan, P.; Fromme, P.; Witt, H. T.; Klukas, O.; Saenger, W.; Krauss, N. Three-Dimensional Structure of Cyanobacterial Photosystem I at 2.5 Å Resolution. *Nature* **2001**, *411* (6840), 909−17.

(9) Cashman, D. J.; Zhu, T.; Simmerman, R. F.; Scott, C.; Bruce, B. D.; Baudry, J. Molecular Interactions Between Photosystem I and Ferredoxin: An Integrated Energy Frustration and Experimental Model. *J. Mol. Recognit.* **2014**, *27* (10), 597−608.

(10) Setif, P.; Harris, N.; Lagoutte, B.; Dotson, S.; Weinberger, S. R. Detection of the Photosystem I: Ferredoxin Complex by Backscattering Interferometry. *J. Am. Chem. Soc.* **2010**, *132* (31), 10620−2.

(11) Bottin, H.; Hanley, J.; Lagoutte, B. Role of Acidic Amino Acid Residues of PsaD Subunit on Limiting the Affinity of Photosystem I For Ferredoxin. *Biochem. Biophys. Res. Commun.* **2001**, *287* (4), 833−6.

(12) Lelong, C.; Boekema, E. J.; Kruip, J.; Bottin, H.; Rogner, M.; Setif, P. Characterization of a Redox Active Cross-Linked Complex Between Cyanobacterial Photosystem I and Soluble Ferredoxin. *EMBO J.* **1996**, *15* (9), 2160−2168.

(13) Lelong, C.; Setif, P.; Lagoutte, B.; Bottin, H. Identification of the Amino-Acids Involved in the Functional Interaction Between Photosystem-I and Ferredoxin from Synechocystis sp. PCC 6803 by Chemical Cross-Linking. *J. Biol. Chem.* **1994**, *269* (13), 10034−10039.

(14) Onuchic, J. N.; Luthey-Schulten, Z.; Wolynes, P. G. Theory of Protein Folding: The Energy Landscape Perspective. *Annu. Rev. Phys. Chem.* **1997**, *48*, 545−600.

(15) Jenik, M.; Parra, R. G.; Radusky, L. G.; Turjanski, A.; Wolynes, P. G.; Ferreiro, D. U. Protein Frustratometer: A Tool to Localize Energetic Frustration in Protein Molecules. *Nucleic Acids Res.* **2012**, *40* (Web Server issue), W348−51.

(16) Lichtarge, O.; Bourne, H. R.; Cohen, F. E. Evolutionarily Conserved Galphabetagamma Binding Surfaces Support a Model of the G Protein-Receptor Complex. *Proc. Natl. Acad. Sci. U. S. A.* **1996**, *93* (15), 7507−11.
(17) Lichtarge, O.; Bourne, H. R.; Cohen, F. E. An Evolutionary Trace Method Defines Binding Surfaces Common to Protein Families. *J. Mol. Biol.* **1996**, *257* (2), 342−58.
(18) Noel, J. K.; Morcos, F.; Onuchic, J. N. Sequence Co-Evolutionary Information is a Natural Partner to Minimally-Frustrated Models of Biomolecular Dynamics. *F1000Research* **2016**, *5*, F1000 Faculty Rev-106.
(19) Bernstein, F. C.; Koetzle, T. F.; Williams, G. J.; Meyer, E. F., Jr.; Brice, M. D.; Rodgers, J. R.; Kennard, O.; Shimanouchi, T.; Tasumi, M. The Protein Data Bank. A Computer-Based Archival File For Macromolecular Structures. *Eur. J. Biochem.* **1977**, *80* (2), 319−24.
(20) Cheatham, T. E., 3rd; Cieplak, P.; Kollman, P. A. A Modified Version of the Cornell et al. Force Field With Improved Sugar Pucker Phases and Helical Repeat. *J. Biomol. Struct. Dyn.* **1999**, *16* (4), 845−62.
(21) Fischer, N.; Setif, P.; Rochaix, J. D. Site-Directed Mutagenesis of the PsaC Subunit of Photosystem I. F(b) is the Cluster Interacting With Soluble Ferredoxin. *J. Biol. Chem.* **1999**, *274* (33), 23333−40.
(22) Setif, P.; Fischer, N.; Lagoutte, B.; Bottin, H.; Rochaix, J. D. The Ferredoxin Docking Site of Photosystem I. *Biochim. Biophys. Acta, Bioenerg.* **2002**, *1555* (1−3), 204−9.
(23) Kozakov, D.; Beglov, D.; Bohnuud, T.; Mottarella, S. E.; Xia, B.; Hall, D. R.; Vajda, S. How Good is Automated Protein Docking? *Proteins: Struct., Funct., Genet.* **2013**, *81* (12), 2159−66.
(24) Kozakov, D.; Brenke, R.; Comeau, S. R.; Vajda, S. PIPER: An FFT-Based Protein Docking Program With Pairwise Potentials. *Proteins: Struct., Funct., Genet.* **2006**, *65* (2), 392−406.
(25) MacKerell, A. D.; Bashford, D.; Bellott, M.; Dunbrack, R. L.; Evanseck, J. D.; Field, M. J.; Fischer, S.; Gao, J.; Guo, H.; Ha, S.; et al. All-Atom Empirical Potential For Molecular Modeling and Dynamics Studies of Proteins. *J. Phys. Chem. B* **1998**, *102* (18), 3586−616.
(26) Amunts, A.; Drory, O.; Nelson, N. The Structure of a Plant Photosystem I Supercomplex at 3.4 Å Resolution. *Nature* **2007**, *447* (7140), 58−63.
(27) Amunts, A.; Toporik, H.; Borovikova, A.; Nelson, N. Structure Determination and Improved Model of Plant Photosystem I. *J. Biol. Chem.* **2010**, *285* (5), 3478−86.
(28) Chapman, H. N.; Fromme, P.; Barty, A.; White, T. A.; Kirian, R. A.; Aquila, A.; Hunter, M. S.; Schulz, J.; DePonte, D. P.; Weierstall, U.; et al. Femtosecond X-Ray Protein Nanocrystallography. *Nature* **2011**, *470* (7332), 73−81.
(29) Brunger, A. T.; Adams, P. D.; Fromme, P.; Fromme, R.; Levitt, M.; Schroder, G. F. Improving the Accuracy of Macromolecular Structure Refinement at 7 Angstrom Resolution. *Structure* **2012**, *20* (6), 957−966.
(30) Page, C. C.; Moser, C. C.; Chen, X. X.; Dutton, P. L. Natural Engineering Principles of Electron Tunnelling in Biological Oxidation-Reduction. *Nature* **1999**, *402* (6757), 47−52.
(31) Fischer, N.; Hippler, M.; Setif, P.; Jacquot, J. P.; Rochaix, J. D. The PsaC Subunit of Photosystem I Provides An Essential Lysine Residue For Fast Electron Transfer to Ferredoxin. *EMBO J.* **1998**, *17* (4), 849−58.
(32) Setif, P. Q.; Bottin, H. Laser Flash Absorption Spectroscopy Study of Ferredoxin Reduction by Photosystem I in Synechocystis sp. PCC 6803: Evidence For Submicrosecond and Microsecond Kinetics. *Biochemistry* **1994**, *33* (28), 8495−504.
(33) Moser, C. C.; Keske, J. M.; Warncke, K.; Farid, R. S.; Dutton, P. L. Nature of Biological Electron Transfer. *Nature* **1992**, *355*, 796−802.
(34) Northrup, S. H.; Thomasson, K. A.; Miller, C. M.; Barker, P. D.; Eltis, L. D.; Guillemette, J. G.; Inglis, S. C.; Mauk, A. G. Effects of Charged Amino Acid Mutations on the Bimolecular Kinetics of Reduction of Yeast iso-1-Ferricytochrome c by Bovine Ferrocytochrome b5. *Biochemistry* **1993**, *32* (26), 6613−23.
(35) Mauk, M. R.; Mauk, A. G.; Weber, P. C.; Matthew, J. B. Electrostatic Analysis of the Interaction of Cytochrome c With Native and Dimethyl Ester Heme Substituted Cytochrome b5. *Biochemistry* **1986**, *25* (22), 7085−91.
(36) Weber, P. C.; Tollin, G. Electrostatic Interactions During Electron Transfer Reactions Between C-Type Cytochromes and Flavodoxin. *J. Biol. Chem.* **1985**, *260* (9), 5568−73.
(37) Chitnis, V. P.; Chitnis, P. R. PsaL Subunit is Required for the Formation of Photosystem I Trimers in the Cyanobacterium Synechocystis sp. PCC 6803. *FEBS Lett.* **1993**, *336* (2), 330−4.

DOI: 10.1021/acs.jpcb.7b08307
J. Phys. Chem. B 2018, 122, 1026−1036